Macromolecular Research

Article

DOI 10.1007/s13233-018-6067-3

www.springer.com/13233 pISSN 1598-5032 eISSN 2092-7673

Functional Graphene Oxide-Based Nanosheets for Photothermal Therapy

Jae Hyun Lim[1]
Da Eun Kim[2]
Eun-Joong Kim[1]
Christian D. Ahrberg[1]
Bong Geun Chung*,[1]

[1] Department of Mechanical Engineering, Sogang University, Seoul 04107, Korea
[2] Department of Biomedical Engineering, Sogang University, Seoul 04107, Korea

Received November 9, 2017 / Revised December 29, 2017 / Accepted December 29, 2017

Abstract: Cancer is one of the main causes of morbidity and mortality. Although a number of techniques are available for treatment, these methods still have a number of drawbacks, destroying healthy tissues and cells to cause various side effects. Here we present the synthesis and biological application of a composite nanomaterial, folic acid (FA)-conjugated graphene oxide (GO) nanosheets functionalized with manganese dioxide (MnO_2) nanoparticles. While FA-conjugated GO nanosheets can be used for targeted photothermal therapy (PTT) when irradiated with a near infrared (NIR) light, MnO_2 nanoparticles degrade hydrogen peroxide (H_2O_2) in the cancer microenvironment, countering hypoxia. Further the nanoparticles can be used as a contrast agent in MRI imaging. We demonstrated that MnO_2-FA-GO nanosheets were uptaken by HeLa cells overexpressing FA receptors to induce NIR irradiation-mediated hyperthermia (35% viability). Therefore, this composite MnO_2-FA-GO nanosheet could be a powerful carrier for cancer targeting and PTT applications.

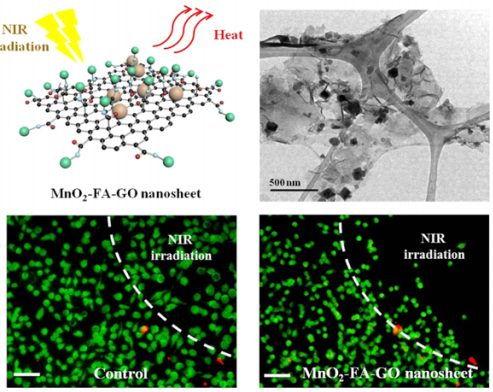

Keywords: graphene oxide nanosheet, photothermal therapy, cancer.

1. Introduction

With 14 million new cases and 8 million cancer related death in 2012, cancer is one of the major causes of morbidity and mortality.[1] Currently, surgery, chemotherapy, and radiotherapy are used in clinical therapies. However, these conventional methods suffer from various drawbacks, such as damaging healthy tissues, attacking the immune system, and increasing the risk of the development of secondary cancers.[2,3] Hypoxia, which is a decrease in the oxygen level in the tissue, is a common characteristic of tumor tissues. It influences proliferation, angiogenesis, and metastasis[4] as well as increases the resistance of the cancer against radio- and chemotherapy.[5-7] Due to these drawbacks, a number of researchers have been motivated to seek for alternative treatment methods. One promising option is hyperthermia, where the target tissue is exposed to high temperatures compared to the surrounding healthy tissues.[8] The cancer cells can directly be destroyed by thermal ablation with temperatures above 47 °C. Alternatively, the temperature can be raised to 41-45 °C, increasing the cancer cells susceptibility to other treatments, by increasing blood flow to the tissue countering hypoxia. A common method of applying heat to the target tissue is photothermal therapy (PTT) in which a photosensitizer (PS) is excited by light, releasing heat in the surrounding matrix through vibrational energy.

Nanomaterials are a promising candidate for cancer treatment due to their unique properties (*e.g.*, small size, biocompatibility, and optical property). Furthermore, the use of nanomaterials could significantly reduce the cost of treatment.[9] Nanoparticles can also be used for PTT as light can induce resonance of free electrons through surface plasmon resonance (SPR). The absorption wavelength of the materials can be tuned to the optical window in the near infrared (NIR) (650-900 nm wavelength) to ensure deep penetration of tissues.[10] Gold nanoshells have previously been used for PTT due to their tunable absorption wavelength of NIR irradiation.[11] In addition, gold nanospheres,[12] nanorods,[13] and nanodrites[14] have been employed for PTT applications. Apart from gold, other materials (*e.g.*, $NaY(MoO_4)_2$ nanorods[15] or magnetic nanoparticles extracted from the magnetic bacterium *Magnetospirillum magneticum*[16]) have previously been developed. Graphene is quickly becoming an alternative to conventional nanomaterials, due to its large surface area, chemical and mechanical stability as well as biocompatibility.[17] Furthermore, graphene can easily be gained from graphite and features high absorption in the NIR range due to the partially restored aromaticity of the graphene sheets.[18] PTT can be combined with chemotherapy or photodynamic therapy (PDT) by binding the PS or drug directly to the reduced graphene oxide (rGO) nanosheets.

Acknowledgments: This research was supported by a grant of the Korea Health Technology R&D Project through the Korea Health Industry Development Institute, funded by the Ministry of Health & Welfare, Republic of Korea (Grant number HI14C3347). This research was supported by the Bio & Medical Technology Development Program of the National Research Foundation (NRF) funded by the Ministry of Science and ICT (MSIT) (Grant number 2015M3A9D7030461). This work was also supported by Leading Foreign Research Institute Recruitment Program through the NRF funded by the MSIT (Grant number 2013K1A4A3055268).

***Corresponding Author:** Bong Geun Chung (bchung@sogang.ac.kr)

For example, doxorubicin can be bounded to rGO and selectively released when the material is heated by NIR irradiation.[19] In combined PDT and PTT, $CuInS_2$/ZnS nanocrystals were incorporated into rGO nanosheets by Wu *et al.*[20] This leads to a decrease in toxicity of the nanocrystals, while the PTT efficiency was increased. $BaGdF_5$ nanoparticles fixed on graphene oxide (GO) nanosheets were used as a contrast reagent for magnetic resonance imaging (MRI) and computer tomography (CT) in other demonstrations of composite nanomaterials.[21,22]

Alternatively, manganese oxide nanoparticles attached to carbon nanotubes can be used for PTT combined with a contrast agent for MRI applications.[23] In addition to acting as a contrasting agent for MRI, manganese dioxide (MnO_2) nanoparticles can also be used for alleviating hypoxia by decomposing hydrogen peroxide (H_2O_2) in the cancer into O_2.[24] Although nanomaterials are a promising carrier for active compounds for cancer treatment capable of controlled release,[25,26] chemicals used for PTT, PDT, and chemotherapy often accumulate in healthy tissues of the patient which can cause to side effects. To reduce these side effects, several different targeting strategies are available leading to a more selective targeting of cancer cells of the active compound.[27,28] Arginine-glycine-aspartic acid (RGD) peptide has been used to target cancer cells by targeting the $\alpha_v\beta_3$ recognition.[29,30] Passive accumulation of MnO_2 hybrid nanoparticles in cancer cells *via* enhanced permeability and retention effect was achieved by Gordijo *et al.*[31] By covering the nanoparticles with a graft terpolymer, the hydrophobicity of the material could be tailored, limiting the decomposition of H_2O_2 to the cancer environment. Alternatively, the folate receptor-mediated endocytosis can be used to deliver macromolecules and nanoparticles into cells by covalently linking them to folic acid (FA).[32] Since receptors for FA are typically overexpressed on human cancer cells, targeting can be achieved with this method.[33] It has previously been used to target cancer cells with Mn-ZnS quantum dots,[34] quercetin-loaded mesoporous silica nanoparticles,[35] and doxorubicin-loaded liposomes.[36] Here, we present the synthesis of GO nanosheets functionalized with FA and MnO_2 nanoparticles. GO can be used as a PS for PTT applications with its absorption characteristics in the NIR window of tissues. The MnO_2 nanoparticles alleviate hypoxia in cancer cells reducing immunity towards conventional drugs used in chemotherapy and PDT applications, while destabilizing the hypoxia-inducible-factor-1alpha (HIF-1α). Further they can be used as a contrast agent in MRI imaging. The FA-conjugation of the nanomaterial allows for a targeting of cancer cells with the material reducing possible side effects on healthy tissues during PTT applications.

2. Experimental

2.1. GO synthesis

GO was prepared through a modified Hummer's method.[19,37] Briefly, 1 g of graphite flakes (Sigma Aldrich, USA) was ground with 50 g of NaCl (Samchun, Korea) for 15 min. The resulting powder was mixed with deionized (DI) water, filtered to remove the sodium chloride, and dried in an oven at 80 °C overnight. The dried graphite flakes were mixed with 50 mL of a sulfuric acid (Duksan, Korea)/phosphoric acid (Sigma Aldrich, USA) (9:1) mixture and 6 g of potassium permanganate (Junsei, Japan) at 0 °C for 8 h. Afterwards the solution was warmed to 40 °C for 30 min and subsequently to 68-80 °C for 1 h. Addition of 50 mL DI water led to a temperature increase to 100 °C. Under vigorous stirring, 150 mL of DI water was added, followed by the addition of 10 mL of 35 v% H_2O_2 solution (Duksan, Korea). The powder was washed three times with 5 v% HCl-solution (Duksan, Korea) and centrifuged at 4,690 rpm for 10 min before freeze drying. Prior to functionalization, the GO was exfoliated using sonication (500 kHz, 2 h) in DI water.

2.2. Surface modification of GO

For surface modification, 50 mL exfoliated GO solution (1 mg/mL in DI water) mixed with 5 g chloroacetic acid (Sigma Aldrich, USA) and 6 g of sodium hydroxide (Sigma Aldrich, USA). It was subsequently sonicated for 3 h (300 W) to convert the hydroxyl groups into carboxyl groups. Afterwards the solution was neutralized with DI water and centrifuged. The obtained graphene pellet was suspended in 20 mL of 50 mM methanesulfonic acid (MES) (Sigma Aldrich, USA) in a concentration of 1 mg/mL before adding 100 mg *N*-hydroxysuccinimide (NHS) (Sigma Aldrich, USA) and 50 mg 1-ethyl-3,3-dimethylaminopropyl carbonodiimide (EDC) (Sigma Aldrich, USA). After sonication (300 W) for 1 h, 100 mg of FA (Sigma Aldrich, USA) was added to the solution and stirred overnight at room temperature. The resulting solution was centrifuged and the supernatant was removed. Afterwards the remaining pellet was freeze dried overnight to obtain a FA-modified GO powder.

2.3. Synthesis of MnO_2 nanoparticles on FA-GO nanosheets

50 mg FA-GO nanosheets were diluted in 100 mL of 1 M NaOH solution (Sigma Aldrich, USA) and sonicated (300 W) for 2 h before dialyzing the solution three times against DI water (3.5-5.0 kDa membrane, Spectrumlabs, USA). Nanoparticles were synthesized by chemical precipitation similar to ZnO nanoparticles previously synthesized on GO.[38] Afterwards 100 mg of $Mn(NO_3)_2$ hydride (Sigma Aldrich, USA) was added and the solution was stirred at room temperature for 24 h for ion exchange. The resulting solution was dialyzed again to remove salts and 6 mL of 3 M NaOH solution (Sigma Aldrich, USA) was added. The solution was stirred at 60 °C for 6 h. In a final dialysis step against DI water (3.5-5.0 kDa tube membrane), the mixture was washed before freeze drying to obtain MnO_2 nanoparticles covalently bound FA-modified GO (MnO_2-FA-GO) nanosheets.

2.4. Characterization of MnO_2-FA-GO nanosheets

Morphologies of GO, FA-GO, and MnO_2-FA-GO nanosheets were confirmed by transmission electron microscopy (TEM) with an accelerating voltage of 200 kV (JEM1100F, JEOL Ltd., Japan). Fourier transformed-infrared (FT-IR, Vertex 70, Bruker, USA) and Raman spectra (LabRam Aramis, Horriba Jovin Yvon, Japan) as well as UV-visible spectra (UV-1800, Shimadzu, Japan) were analyzed for all three materials. Surface charges were determined

using dynamic light scattering (Zetasizer, Malvern Instruments Ltd., United Kingdom). The photothermal effect was characterized by illuminating samples with a NIR laser (808 nm, 5 W/cm^2, BWF2, B&W, USA) and recording the temperature of the solution every 60 seconds using a temperature sensor (DTM-318, Tecpel Co. Ltd., Taiwan). T_1-weighted MRI phantom images of MnO_2-FA-GO solutions with various concentrations of MnO_2-FA-GO nanosheets were acquired using a 9.4 T (400 MHz) MRI scanner (Agilent Technologies, USA). The following MRI parameters were used: eco time (TE) of 8.71 ms, repetition time (TR) of 500 ms, matrix size of 192×192, field of view (FOV) of 60×35 mm, and a slice thickness of 1 mm.

2.5. Degradation of H_2O_2 by MnO_2-FA-GO nanosheets

To observe the ability of the MnO_2-FA-GO nanosheets to degrade H_2O_2, a solution of 30 μg/mL nanosheets in cell culture medium (Life Technologies, USA) was used. The pH of the solution was adjusted to 7.8, 6.8, and 5.8 using hydrochloric acid. 120 μM H_2O_2 (Duksan, Korea) was added and degradation was observed over time using PeroXquant assay kit (Pierce, USA) according to the manufacturer's instructions. Control experiments were conducted using medium without the addition of MnO_2-FA-GO nanosheets.

2.6. Cellular uptake of MnO_2-FA-GO nanosheets

For fluorescence labeling, MnO_2-FA-GO and MnO_2-GO nanosheet solutions with a concentration of 1 mg/mL were mixed with 2 mg/mL fluorescein isothiocyanate (FITC)-labeled dextran (10 kDa, Sigma Aldrich, USA) in DI water. Following stirring overnight, the supernatant was removed after centrifugation and the remaining nanosheets washed with phosphate-buffered saline (PBS) (Intron Biotechnology, Korea) three times. HeLa and NIH3T3 fibroblast cells were seeded (6×10^4 cells/well) into 8-well culture plates (Ibidi, Germany) before treatment with 200 μL of 30 μg/mL fluorescently labeled MnO_2-FA-GO or MnO_2-GO solution in PBS. Then cells were incubated at 37 °C for 5 h, followed by a washing step with PBS. 4% Paraformaldehyde (Sigma Aldrich, USA) was used to fix the cells. After another washing step with PBS, cells were permeabilized using 1% Triton X-100 (Sigma Aldrich, USA) in PBS at room temperature for 15 min and subsequently washed with PBS. After incubation for 2 h at 37 °C, the staining was performed using Alexa Fluor 594 Phalloidin (Thermo Fisher, USA) in PBS for 20 min at 37 °C and 4',6-diamidino-2-phenylindole (DAPI, Thermo Fisher, USA) for 5 min. Finally, the cellular uptake of MnO_2-FA-GO nanosheets was analyzed using confocal laser-scanning microscopy (LSM-710, Carl Zeiss, Germany).

2.7. Fluorescence activated cell counting (FACS) analysis

For quantitative analysis of cellular uptake, the cells were treated with trypsin-ethylenediaminetetraacetic acid (EDTA) (Thermo Fisher Scientific, USA) after initial incubation with the fluorescent-labeled MnO_2-FA-GO nanosheets. Cells were fixed with formaldehyde at room temperature for 30 min. The supernatant was discarded and the cells were dispersed in PBS. The analysis of cellular uptake was performed by FACS (FACS Calibur, BD Bioscience, USA) and results were visualized using the FlowJo software (BD Bioscience, USA). FACS experiments for the quantitative analysis of cellular uptake were conducted in triplicate.

2.8. Toxicity of MnO_2-FA-GO nanosheets

100 μL solution containing 5×10^4 HeLa or NIH3T3 fibroblast cells was seeded in a 96-well plate and incubated at 37 °C for 24 h. Cell culture medium was removed and replaced with 100 μL medium containing MnO_2-FA-GO nanosheets of different concentrations (0-50 μg/mL). After 5 h of incubation, 5 μL of 3-(4,5-dimethylthiazol-2-yl)-2,5-diphenyltetrazolium bromide (MTT)-labelling reagent (Roche, Switzerland) was added and cells were incubated for an additional 4 h. 100 μL of solubilisation reagent (Roche, Switzerland) was added. Cell viability was measured using a spectrophotometrical plate reader (EL800 Microplate Reader, BioTek, USA) after further incubation overnight.

2.9. PTT effect of MnO_2-FA-GO nanosheets

100 μL 5×10^5 HeLa cells were incubated in 96-well plates at 37 °C in a 5% CO_2 incubator overnight. MnO_2-FA-GO nanosheets were added in a concentration of 30 μg/mL and incubated for 5 h. Samples were irradiated with a NIR laser (808 nm, 5 W/cm^2) for 3 min. After NIR irradiation, 5 μL MTT labeling reagent (Roche, Switzerland) was added to each well and cells were incubated for 3 h at 37 °C in a 5% CO_2 incubator. 100 μL MTT solubilisation reagent (Roche, Switzerland) was added and cells were incubated overnight. After controlling complete solubilisation, absorbance was measured using a spectrophotometrical plate reader. Control experiments were conducted without NIR irradiation and without the addition of MnO_2-FA-GO nanosheets. Further live/dead fluorescence images were taken after PTT. For this, 400 μL solution containing 2×10^6 HeLa cells was seeded into confocal culture dishes (SPL Life Science, Korea) and the cells were incubated overnight. The culture medium was removed and replaced with fresh medium containing 30 μg/mL MnO_2-FA-GO nanosheets. After 5 h of further incubation, the cells were washed with PBS (Intron Biotechnology, Korea) and fresh culture medium was added. Samples were irradiated with a NIR laser (808 nm, 5 W/cm^2) for 3 min and washed with PBS. The live/dead staining carried out with live/dead cytotoxicity kit (Thermo Fisher Scientific, USA) according to manufacturer's recommendations. After 40 min of incubation, the cells were washed with PBS and fluorescent microscopy images were taken.

3. Results and discussion

3.1. Synthesis of MnO_2-FA-GO nanosheets

GO nanosheets functionalized with FA and MnO_2 nanoparticles were synthesized from graphite (Figure 1). After preparation of GO nanosheets, functionalization with FA and MnO_2 nanoparticles were synthesized *via* chemical precipitation. This was shown

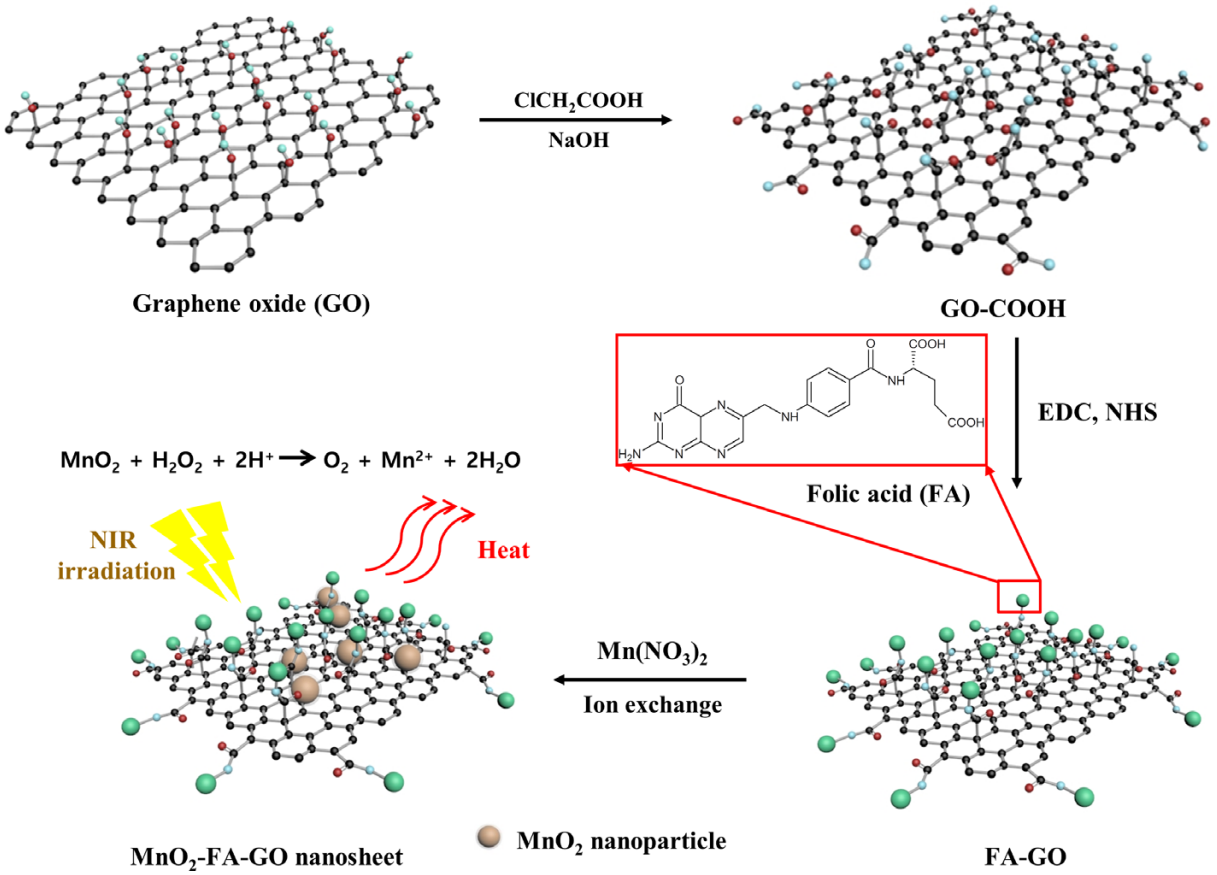

Figure 1. Schematic illustration of the three step synthesis of MnO_2-FA-GO nanosheets. In a first step, rGO nanosheets are modified with carboxylic acid groups. In a second step, FA is attached to the GO nanosheets in a solution containing EDC and NHS. In a last step, an MnO_2 nanoparticles are synthesized by chemical precipitation.

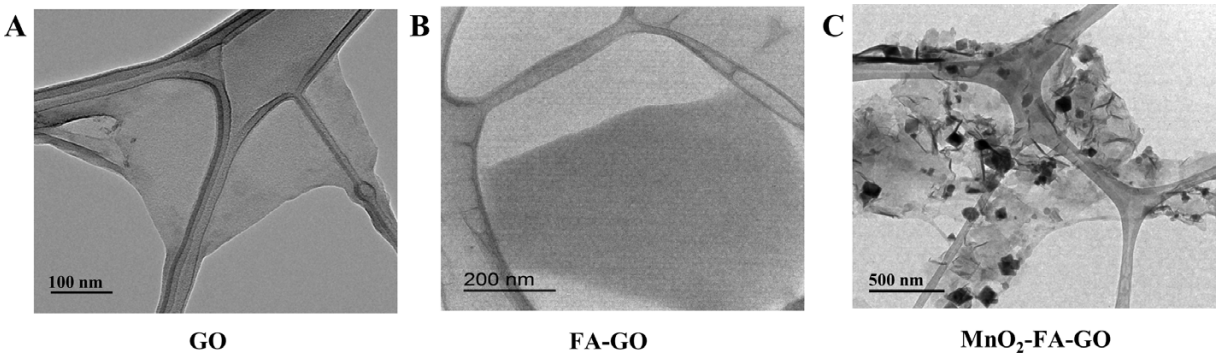

Figure 2. TEM images of GO (A), FA-GO (B), and MnO_2-FA-GO nanosheets (C). GO is recognizable as a grey film on TEM images, while the MnO_2 nanoparticles are visible as black squares.

in TEM images (Figure 2). The light grey layer in TEM images are GO nanosheets. As can be seen from the comparison of Figure 2(A) and 2(B), the addition of FA to the nanosheets did not lead to a dramatic change visible by TEM. The successful chemical precipitation and synthesis of MnO_2 nanoparticles on the surface of the nanosheet can be concluded from the black square crystals on the GO nanosheets in the TEM image (Figure 2(C)). The average size of GO, GO-COOH, FA-GO and MnO_2-FA-GO nanosheets was measured by DLS analyzer, showing that the size of GO and GO-COOH was approximately 243±26.3 nm and 207±3.9 nm, respectively. The size of FA-GO nanosheet was about 400±4.4 nm. The size of FA-GO nanosheet is larger than GO and GO-COOH, because the carboxylic and amine group of folic acid onto graphene oxide were aggregated by hydrogen bonding. The size of MnO_2-FA-GO nanosheet is approximately 155±3.9 nm. The size of MnO_2-FA-GO nanosheet is smaller than the size of FA-GO nanosheet, because MnO_2 nanoparticles formed by ion exchange interrupted hydrogen bonding between carboxylic and amine group of FA-GO nanosheet. The average size of MnO_2 nanoparticles on the GO nanosheets is approximately 15.3±2.9 nm.

3.2. Analysis of MnO_2-FA-GO nanosheets

FTIR spectra, Raman spectra, and UV-visible spectra were analyzed (Figure 3(A)-(C)). In the FTIR spectrum of GO (Figure 3(A)), characteristic peaks can be seen at 3,370 nm, corresponding to

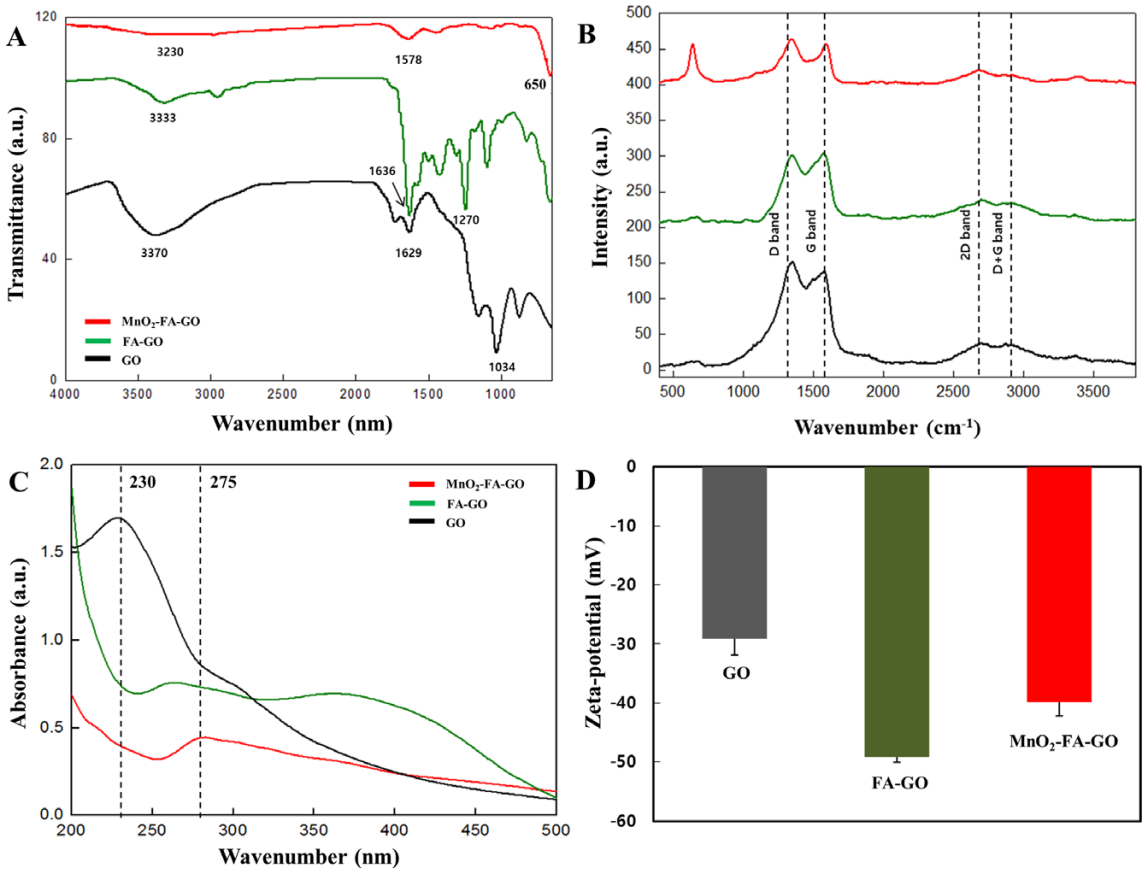

Figure 3. FT-IR spectra, Raman spectra, UV-visible spectra, and Zeta potentials of GO, FA-GO, and MnO_2-FA-GO nanosheets. (A) Analysis of FT-IR spectra. (B) Raman spectra show the G and D bands of GO at 1574 cm^{-1} and 1350 cm^{-1} (MnO_2-FA-GO: red line, FA-GO: green line, GO: black line). (C) UV-visible spectra confirm the presence of GO (peak at 275 nm) and the MnO_2 nanoparticles (absorption band between 370 and 430 nm). (D) Analysis of Zeta potentials.

-OH vibrations, and 1,629 nm, C=C stretching vibrations. Peaks with the same wavelength have previously been reported for a GO sandwich material for applications in supercapacitors.[39] Characteristic peaks at 3,333 nm and 1,270 nm, corresponding to OH and C-N vibrations, indicated the successful addition of FA. Similar peaks have also been described by Muhammad *et al.* who functionalized ZnO quantum dots with FA.[40] The transmittance intensity of 1,730 nm of GO and FA-GO is lower than 1,629 nm range, as previously described.[41] FA was conjugated with GO-COOH using EDC/NHS coupling, showing that -carboxylic position of FA was conjugated with GO-COOH surface. Thus, 1,730 nm intensity of FA-GO nanosheets is lower than GO nanosheets. The addition of MnO_2 nanoparticles leads to a slight shift in peaks as observed by Han *et al.* for GO-MnO_2 sandwich materials.[39] Furthermore, an absorption band at 650 nm indicates successful synthesis of the MnO_2 nanoparticles onto FA-GO nanosheets. All Raman spectra show two distinct peaks (Figure 3(B)). The first peak at 1,574 cm^{-1} is the G band, corresponding to sp^2-hybridized carbon-carbon bonds, while the second peak at 1,350 cm^{-1}, the D band, originating from lattice disorder of GO. These peaks are characteristic for GO monolayers as previously described.[42] This confirms the presence of GO during all steps of the synthesis. In the UV-visible spectra, the original absorption peak of GO at 230 nm shifts to a wavelength of 275 nm through the attachment of FA to GO nanosheets (Figure 3(C)), as reported by P. Huang *et al.* who described FA-conjugated GO as a carrier for PS for PDT applications.[43] The attachment of MnO_2 nanoparticles to the FA-GO nanosheets can be deducted from the increased absorption developing between 370 and 430 nm in the UV-visible spectrum, which is similar wavelength to the absorption band found for colloidal manganese dioxide.[44] Zeta potentials were measured for the nanomaterials (Figure 3(D)). For all materials, negative zeta-potentials were found with GO, having the smallest at -29 mV. FA-GO and MnO_2-FA-GO nanosheets have larger Zeta-potentials at -49 and -40 mV, respectively. This indicates that MnO_2-FA-GO nanosheets have good stability and are resistant against aggregation. The possibility of manganese-related MRI imaging was tested with T_1-weighted MRI phantom images. A brighter, dose dependent contrast was observed in MRI images (Supplemental Figure S1). Hence, the MnO_2-FA-GO nanosheets could be used as a potential T_1 MRI contrast agent.

3.3. PTT properties of MnO_2-FA-GO nanosheets

PTT properties of the synthesized MnO_2-FA-GO nanosheets were tested by irradiating with a NIR laser for 10 min (Figure 4(A)). All nanosheet materials (GO, FA-GO, and MnO_2-FA-GO) display a temperature increase when irradiated by the NIR laser, due to the absorption properties of GO nanosheets. It can be deducted that the FA-GO and MnO_2-FA-GO nanosheets show better PTT

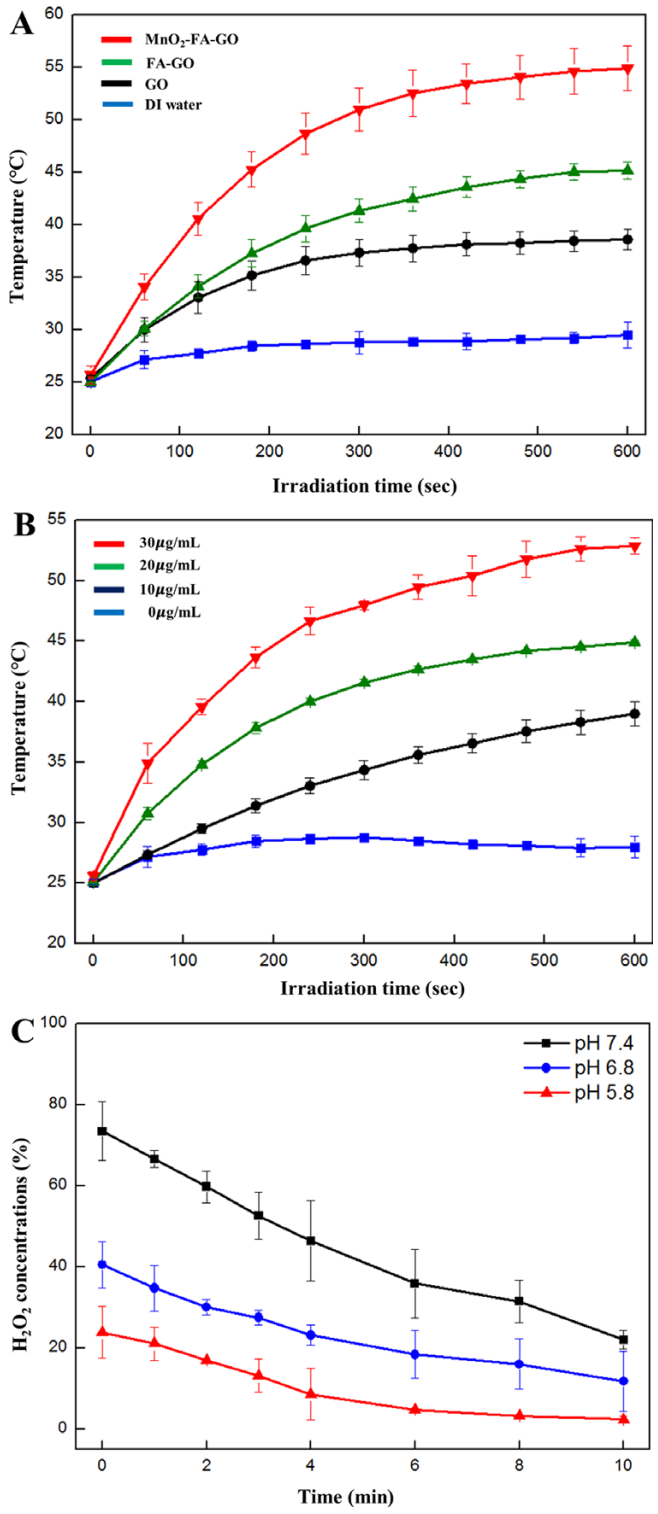

Figure 4. (A) Temperature analysis of GO, FA-GO, and MnO_2-FA-GO nanosheets in solution when irradiated with an NIR laser (808 nm). (B) Temperature analysis of suspensions containing different concentrations of MnO_2-FA-GO nanosheets when irradiated by a NIR laser. (C) Decomposition of H_2O_2, demonstrating the hypoxia reliving properties of MnO_2.

performance than the unmodified GO with temperature increases of 20 °C and 30 °C after 10 min of NIR irradiation. A possible explanation for this observed effect might be energy transfer in the modified GO material.[45,46] Also, the concentration of MnO_2-FA-GO nanosheets required to obtain a temperature above 47 °C, which is required for thermal ablation, was tested (Figure 4(B)). The required temperature can be achieved with a concentration of 30 μg/mL MnO_2-FA-GO nanosheets after 3.5 min of NIR irradiation starting from room temperature. Concentrations lower than 30 μg/mL are not able to reach the temperature required for thermal ablation, while higher concentrations could accelerate the heating rate. However, with a concentration of nanosheets of 30 μg/mL, temperatures of 47 °C can be reached in less than 5 min, which would be suitable for PTT applications.

3.4. Degradation of H_2O_2 by MnO_2-FA-GO nanosheets

We demonstrated the ability of MnO_2-FA-GO nanosheets to degrade H_2O_2 (Figure 4(C)). Experiments were conducted in cell culture medium with a pH adjusted to 7.4, 6.8, and 5.5. Under all pH conditions, fast degradation of H_2O_2 was observed due to the large surface area of the MnO_2 nanoparticles on the GO nanosheets. Two protons are consumed for every peroxide molecule consumed. Thus, the faster degradation of peroxide that was observed in acidic conditions could be expected from the reaction kinetics. The initial concentration of H_2O_2 measured did not correspond to the prepared concentrations. This is caused by the fast initial reaction, decomposing significant amounts of H_2O_2 in the short time period between preparing samples and the first measurement of concentration. Gordijo *et al.* have reported degradation of H_2O_2 by embedded polyelectrolyte-MnO_2 nanoparticles in suspension.[31] They observed fast degradation rates with complete degradation of H_2O_2 in less than 10 min. Here, we have observed similar rates and complete degradation in the same time, indicating that the reactivity of the MnO_2 nanoparticles has not been reduced by the attachment to the GO nanosheets.

3.5. Cellular uptake of MnO_2-FA-GO nanosheets

Nanomaterial uptake was tested with HeLa and NIH3T3 fibroblast cells by treating the cells with fluorescent-labeled MnO_2-FA-GO nanosheets. To evaluate the influence of FA on the uptake properties, control experiments were conducted with fluorescent-labeled MnO_2-GO nanosheets. The cellular uptake was analyzed using laser scanning confocal microscopy (Figure 5) and FACS (Figure 6). From the confocal microscopy images, it can be observed that HeLa cells readily take up the nanosheets (Figure 5(C)), while the uptake efficiency of NIH3T3 fibroblast cells is significantly lower (Figure 5(F)). As suggested by Torrano *et al.*,[47] confocal z-stack images were taken to confirm uptake of MnO_2-FA-GO nanosheets into the cells (Supplemental Figure S2). Scanning through a single HeLa cell from bottom to top, it can be seen that a majority of the nanosheets accumulates inside the cytosol of the HeLa cells. In comparison to the FA-conjugated nanosheets, uptake of nanosheets without FA conjugation could not be observed in NIH3T3 fibroblast cells (Figure 5(E)), while only single HeLa cells took up small amounts of nanosheets (Figure 5(B)). This indicates the importance of the folate receptor endocytosis for the uptake of the nanosheets. As NIH3T3 fibroblast cells are negative for the folate receptor, less uptake was observed. The fluorescent images display no morphological

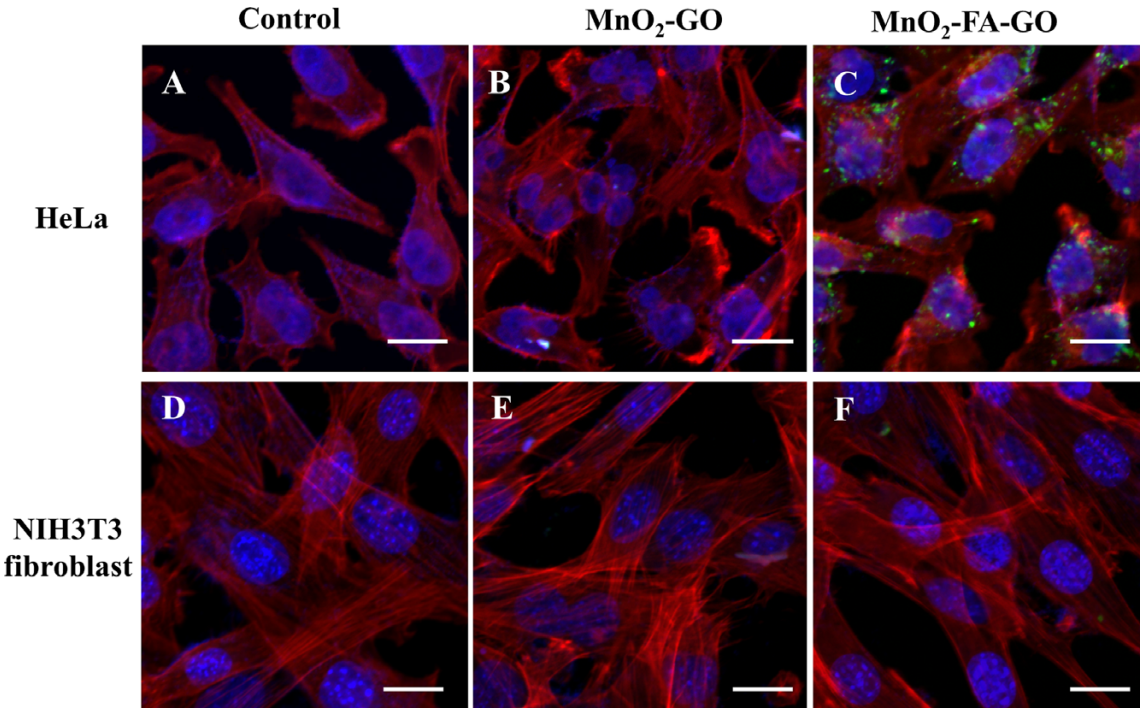

Figure 5. Confocal fluorescence microscope images of cellular uptake of MnO_2-FA-GO nanosheets by HeLa cells and NIH3T3 fibroblast cells. MnO_2-FA-GO Nanosheets are stained in green, cell membranes in red, and cell nuclei in blue. Control experiment of HeLa cells without nanosheets (A), HeLa cells incubated with 30 μg/mL MnO_2-GO nanosheets (B), and HeLa cells incubated with 30 μg/mL MnO_2-FA-GO nanosheets (C). Control experiment with FA-negative NIH3T3 fibroblast cells (D), NIH3T3 fibroblast cells incubated with 30 μg/mL MnO_2-GO nanosheets (E), and NIH3T3 fibroblast cells incubated with 30 μg/mL MnO_2-FA-GO nanosheets (F). Scale bars are 20 μm.

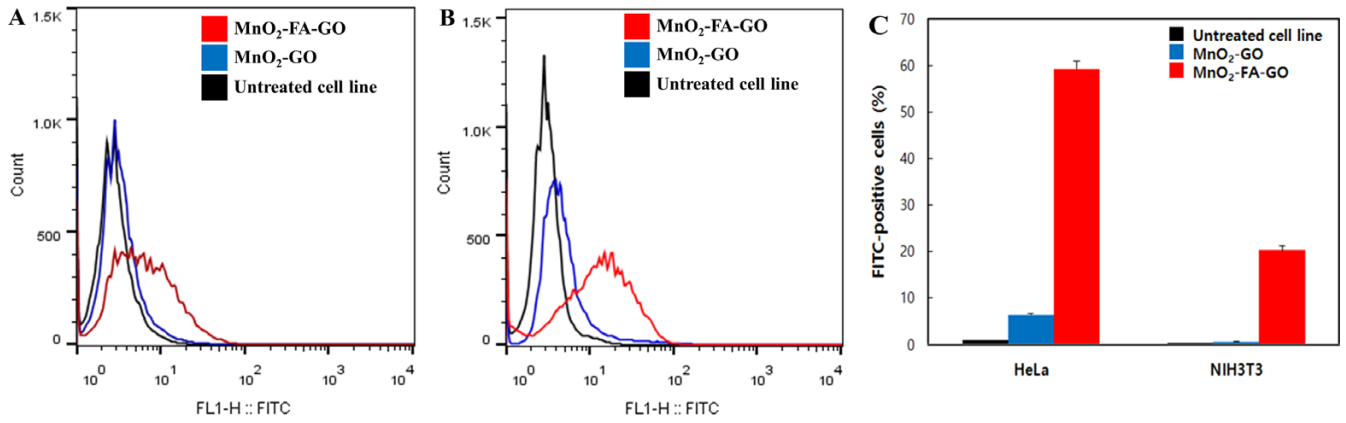

Figure 6. Cellular uptake of MnO_2-FA-GO nanosheets as quantified by FACS analysis. Uptake of nanosheets in control of NIH3T3 fibroblast cells (A) and HeLa cells (B). Fractions of cells displaying uptake of the fluorescent-labelled MnO_2-FA-GO nanosheets (C).

difference between treated and untreated cells (Figure 5(A),(D)). For quantitative assessment of nanosheet uptake, FACS analysis was performed (Figure 6). The threshold fluorescence for uptake was defined from the untreated cell peak in a manner that 99% of the untreated cells are below the fluorescence threshold value. As expected from confocal microscopy images, the MnO_2-GO nanosheets without FA modification show only low uptake by both cell types. FA-conjugated nanosheets, in contrast, were uptaken by a significant portion of HeLa cells (Figure 6(B)), while a smaller fraction of NIH3T3 fibroblast cells displayed uptake of the MnO_2-FA-GO nanosheets (Figure 6(A)). While almost 60% of HeLa cells display uptake of the MnO_2-FA-GO nanosheets, only 20% uptake is shown in FA receptor-negative NIH3T3 fibroblast cells (Figure 6(C)). This illustrates how targeting can be achieved through FA modification of the MnO_2-FA-GO nanosheets utilizing the receptor-mediated endocytosis of the overexpressed folate receptors on HeLa cells.

3.6. Toxicity of MnO_2-FA-GO nanosheets

The toxicity of the MnO_2-FA-GO nanosheets was tested using a MTT assay (Supplemental Figure S3). After 24 h, the viability of NIH3T3 fibroblast cells was higher compared to a low viability of HeLa cells. This is a consequence of the NIH3T3 fibroblast cells taking up less of the MnO_2-FA-GO nanosheets compared to HeLa cells. After 24 h, a cell viability of more than 80% could be observed

for NIH3T3 fibroblast cells for MnO_2-FA-GO nanosheet concentrations of up to 50 μg/mL, while those of HeLa cells were lower at around 65% for the same concentration range. Hence, the toxicity of the MnO_2-FA-GO nanosheets is comparable to the toxicity reported for recently presented rGO-conjugated with $CuInS_2$/ZnS nanocrystals[20] and gadolinium polytungstate nanoclusters used for PTT combined with dual mode of MRI/CT imaging.[48]

3.7. PTT applications of MnO_2-FA-GO nanosheets

The MnO_2-FA-GO nanosheets were tested in *in vitro* testing of PTT effect using HeLa cells (Figure 7). First, the PTT effect of the MnO_2-FA-GO nanosheets was assessed qualitatively (Figure 7(A)). In control experiments without MnO_2-FA-GO nanosheets, no difference in cell viability before and after NIR irradiation could be observed. In contrast, when the MnO_2-FA-GO nanosheets were applied, the cells within the irradiation area of the NIR laser died during the PTT treatment, while cells outside of the irradiation area remained viable due to endocytosis of MnO_2-FA-GO nanosheets. Second, MTT assays were conducted to quantify the PTT effect of the MnO_2-FA-GO nanosheets (Figure 7(B)). The NIR irradiation in control experiments did not adversely affect viability of HeLa cells. Addition of nanosheets, however,

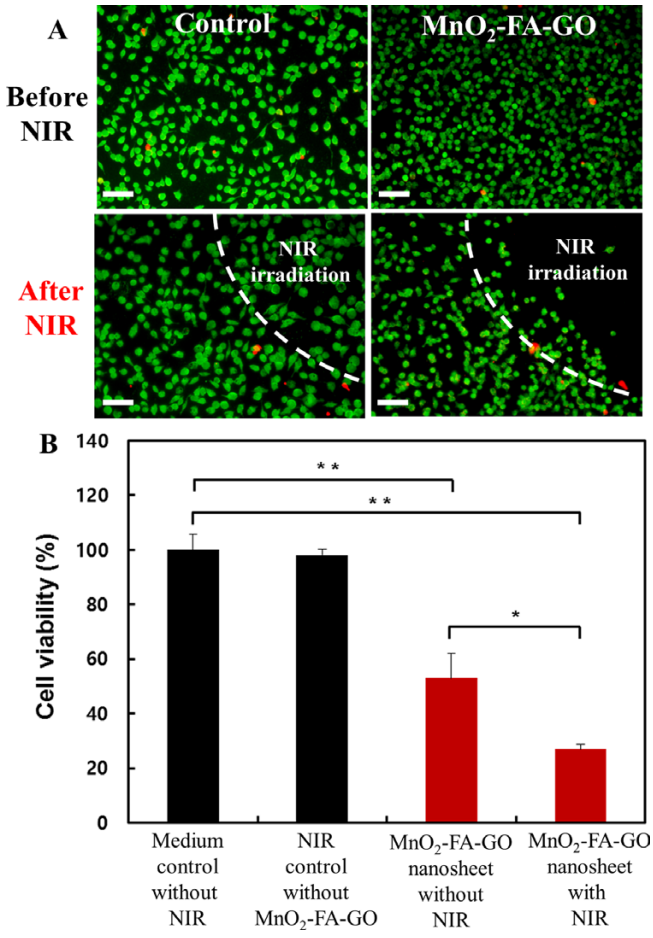

Figure 7. Analysis of PTT experiments employing the MnO_2-FA-GO nanosheets in HeLa cells. Live (green)/dead (red) fluorescence images of HeLa cells before and after NIR irradiation with 30 μg/mL MnO_2-FA-GO nanosheets (A). Scale bars are 100 μm. MTT analysis of PTT experiments with 30 μg/mL MnO_2-FA-GO nanosheets (B) (*p<0.05, **p<0.01).

leads to a decrease in cell viability before NIR irradiation due to the dark-toxicity of the MnO_2-FA-GO nanosheets. The NIR irradiation leads to a significant decrease in cell viability. After only 3 min of irradiation, more than two thirds of the HeLa cells were dead, indicating the usefulness of the MnO_2-FA-GO nanosheets for PTT applications. The increase of temperature is affected by the presence of manganese nanoparticles, as previously described.[49] Surprisingly, in fluorescence images, cell death from the dark toxicity of the nanosheets is not observable in the extent expected from the MTT assays. The cells, which die through the dark toxicity of the nanomaterial, may be detached from the surface of the confocal culture dishes. The dead cells free floating in solution are out of the focal plane of the fluorescent microscope and thus not visible in the images. It might be possible to reduce the dark toxicity of MnO_2-FA-GO nanosheets by modifying the MnO_2 nanoparticles with a polymer matrix material.[31]

4. Conclusions

We synthesized MnO_2-FA-GO composite nanosheets. The GO nanosheets acts as a PS for PTT applications. The cancer cells can be targeted through the FA-conjugation of the MnO_2-FA-GO nanosheets, leading to a faster uptake in HeLa cells overexpressing FA-receptors. MnO_2 nanoparticles attached to the GO nanosheets relive hypoxia in cancers by degrading H_2O_2. Furthermore, they can be used as a contrast agent for MRI imaging applications. Due to the large surface area of the nanosheets, fast degradation of H_2O_2 under different conditions was observed. PTT analysis was also successfully demonstrated that the viability of HeLa cells treated with MnO_2-FA-GO nanosheets and NIR irradiation was significantly decreased. Therefore, this MnO_2-FA-GO composite nanosheet could provide a new efficient method of cancer targeted PTT combined with treatment of hypoxia.

Supporting information: Information is available regarding the MRI images of MnO_2-FA-GO nanosheets, confocal z-stack images of cellular uptake with MnO_2-FA-GO nanosheets, and cytotoxicity analysis of the cells cultured with MnO_2-FA-GO nanosheets. The materials are available *via* the Internet at http://www.springer.com/13233.

References

(1) IARC, *World Cancer Report 2014*, World Health Organization, Lyon, 2014.
(2) F. M. Kievit and M. Zhang, *Acc. Chem. Res.*, **44**, 853 (2011).
(3) C. P. Nolsøe, S. Torp-Pedersen, F. Burcharth, T. Horn, S. Pedersen, N. E. Christensen, E. S. Olldag, P. H. Andersen, S. Karstrup, and T. Lorentzen, *Radiology*, **187**, 333 (1993).
(4) J. A. Bertout, S. A. Patel, and M. C. Simon, *Nat. Rev. Cancer*, **8**, 967 (2008).
(5) S. Masuda and J. C. I. Belmonte, *Nat. Rev. Clin. Oncol.*, **10**, 79 (2013).
(6) M. Milosevic, P. Warde, C. Ménard, P. Chung, A. Toi, A. Ishkanian, M. McLean, M. Pintilie, J. Sykes, M. Gospodarowicz, C. Catton, R. P. Hill, and R. Bristow, *Clin. Cancer Res.*, **18**, 2108 (2012).
(7) T. D. Eubank, R. D. Roberts, M. Khan, J. M. Curry, G. J. Nuovo, P. Kuppusamy, and C. B. Marsh, *Cancer Res.*, **69**, 2133 (2009).
(8) J. Beik, Z. Abed, F. S. Ghoreishi, S. Hosseini-Nami, S. Mehrzadi, A. Shakeri-Zadeh, and S. K. Kamrava, *J. Control. Release*, **235**, 205 (2016).

(9) N. S. Abadeer and C. J. Murphy, *J. Phys. Chem. C*, **120**, 4691 (2016).
(10) R. Weissleder, *Nat. Biotechnol.*, **19**, 316 (2001).
(11) L. R. Hirsch, R. J. Stafford, J. A. Bankson, S. R. Sershen, B. Rivera, R. E. Price, J. D. Hazle, N. J. Halas, and J. L. West, *Proc. Natl. Acad. Sci. U.S.A.*, **100**, 13549 (2003).
(12) I. H. El-Sayed, X. Huang, and M. A. El-Sayed, *Cancer Lett.*, **239**, 129 (2006).
(13) X. Huang, I. H. El-Sayed, W. Qian, and M. A. El-Sayed, *J. Am. Chem. Soc.*, **128**, 2115 (2006).
(14) P. Qiu, M. Yang, X. Qu, Y. Huai, Y. Zhu, and C. Mao, *Biomaterials*, **104**, 138 (2016).
(15) H. Zheng, B. Chen, H. Yu, X. Li, J. Zhang, J. Sun, L. Tong, Z. Wu, H. Zhong, R. Hua, and H. Xia, *Sens. Actuator B-Chem.*, **234**, 286 (2016).
(16) C. Chen, S. Wang, L. Li, P. Wang, C. Chen, Z. Sun, and T. Song, *Biomaterials*, **104**, 352 (2016).
(17) J. Liu, L. Cui, and D. Losic, *Acta Biomater.*, **9**, 9243 (2013).
(18) J. T. Robinson, S. M. Tabakman, Y. Liang, H. Wang, H. Sanchez Casalongue, D. Vinh, and H. Dai, *J. Am. Chem. Soc.*, **133**, 6825 (2011).
(19) Y. A. Cheon, J. H. Bae, and B. G. Chung, *Langmuir*, **32**, 2731 (2016).
(20) Q. Wu, M. Chu, Y. Shao, F. Wo, and D. Shi, *Carbon*, **108**, 21 (2016).
(21) H. Zhang, H. Wu, J. Wang, Y. Yang, D. Wu, Y. Zhang, Y. Zhang, Z. Zhou, and S. Yang, *Biomaterials*, **42**, 66 (2015).
(22) S. Kim, S. M. Ahn, J.-S. Lee, T. S. Kim, and D.-H. Min, *2D Materials*, **4**, 025069 (2017).
(23) S. Wang, Q. Zhang, P. Yang, X. Yu, L.-Y. Huang, S. Shen, and S. Cai, *ACS Appl. Mater. Interfaces*, **8**, 3736 (2016).
(24) M. Song, T. Liu, C. Shi, X. Zhang, and X. Chen, *ACS Nano*, **10**, 633 (2016).
(25) M. Gulfam and B. G. Chung, *Macromol. Res.*, **22**, 412 (2014).
(26) H. I. Seo, A.-N. Cho, J. Jang, D.-W. Kim, S.-W. Cho, and B. G. Chung, *Nanomedidine*, **11**, 1861 (2015).
(27) A.-R. Blaudszun, G. Moldenhauer, M. Schneider, and A. Philippi, *J. Control. Release*, **197**, 58 (2015).
(28) A. M. Bugaj, *Photochem. Photobiol. Sci.*, **10**, 1097 (2011).
(29) F. Danhier, A. L. Breton, and V. Préat, *Mol. Pharm.*, **9**, 2961 (2012).
(30) Y. Hu, L. He, J. Ding, D. Sun, L. Chen, and X. Chen, *Carbohydr. Polym.*, **144**, 223 (2016).
(31) C. R. Gordijo, A. Z. Abbasi, M. A. Amini, H. Y. Lip, A. Maeda, P. Cai, P. J. O'Brien, R. S. DaCosta, A. M. Rauth, and X. Y. Wu, *Adv. Funct. Mater.*, **25**, 1858 (2015).
(32) C. P. Leamon and P. S. Low, *Proc. Natl. Acad. Sci. U.S.A.*, **88**, 5572 (1991).
(33) P. S. Low and S. A. Kularatne, *Curr. Opin. Chem. Biol.*, **13**, 256 (2009).
(34) I. B. Bwatanglang, F. Mohammad, N. A. Yusof, J. Abdullah, N. B. Alitheen, M. Z. Hussein, N. Abu, N. E. Mohammed, N. Nordin, N. R. Zamberi, and S. K. Yeap, *J. Colloid Interface Sci.*, **480**, 146 (2016).
(35) A. Sarkar, S. Ghosh, S. Chowdhury, B. Pandey, and P. C. Sil, *Biochim. Biophys. Acta,* **1860**, 2065 (2016).
(36) S. K. Sriraman, G. Salzano, C. Sarisozen, and V. Torchilin, *Eur. J. Pharm. Biopharm.,* **105**, 40 (2016).
(37) W. S. Hummers and R. E. Offeman, *J. Am. Chem. Soc.*, **80**, 1339 (1958).
(38) Z. Hu, J. Li, C. Li, S. Zhao, N. Li, Y. Wang, F. Wei, L. Chen, and Y. Huang, *J. Mater. Chem. B*, **1**, 5003 (2013).
(39) G. Han, Y. Liu, E. Kan, J. Tang, L. Zhang, H. Wang, and W. Tang, *RSC Adv.*, **4**, 9898 (2014).
(40) F. Muhammad, M. Guo, Y. Guo, W. Qi, F. Qu, F. Sun, H. Zhao, and G. Zhu, *J. Mater. Chem.*, **21**, 13406 (2011).
(41) Sudesh, N. Kumar, S. Das, C. Bernhard, and G. D. Varma, *Supercond. Sci. Technol.*, 2013, **26**, 095008
(42) C.-Y. Su, Y. Xu, W. Zhang, J. Zhao, X. Tang, C.-H. Tsai, and L.-J. Li, *Chem. Mater.*, **21**, 5674 (2009).
(43) P. Huang, C. Xu, J. Lin, C. Wang, X. Wang, C. Zhang, X. Zhou, S. Guo, and D. Cui, *Theranostics*, **1**, 240 (2011).
(44) P. Mulvaney, R. Cooper, F. Grieser, and D. Meisel, *J. Phys. Chem.*, **94**, 8339 (1990).
(45) E. H. M. Sakho, O. S. Oluwafemi, S. Thomas, and N. Kalarikkal, *J. Mater. Sci., Mater. Electron.*, **28**, 2651 (2017).
(46) Z. Chen, S. Berciaud, C. Nuckolls, T. F. Heinz, and L. E. Brus, *ACS Nano*, **4**, 2964 (2010).
(47) A. A. Torrano and C. Bräuchle, *Beilstein J. Nanotechnol.*, **5**, 1616 (2014).
(48) Y. Yong, L. Zhou, S. Zhang, L. Yan, Z. Gu, G. Zhang, and Y. Zhao, *NPG Asia Mater.*, **8**, e273 (2016).
(49) W. W. Zhu, K. Liu, X. Q. Sun, X. Wang, Y. G. Li, L. Cheng, and Z. Liu, *ACS Appl. Mater. Interfaces*, **7**, 11575 (2015).

